Electrochemistry Communications 136 (2022) 107237

Contents lists available at ScienceDirect

Electrochemistry Communications

journal homepage: www.elsevier.com/locate/elecom

Porous ternary Pt-based branched nanostructures for electrocatalytic oxygen reduction

Kamel Eid [a,*], Aboubakr M. Abdullah [b]

[a] Gas Processing Center, College of Engineering, Qatar University, Doha 2713, Qatar
[b] Center for Advanced Materials, Qatar University, Doha 2713, Qatar

ARTICLE INFO

Keywords:
Porous ternary Pt
Branched trimetallic Pt
Pt dendrites
Oxygen reduction reaction
Metal-air battery
Fuel cells

ABSTRACT

The oxygen reduction reaction (ORR) is pivotal for optimizing the energy output of fuel cells and metal-air batteries; however, their commercialization is precluded by the intolerable cost, instability, earth-scarcity of Pt that remains a prestigious catalyst for ORR. Porous ternary Pt-based branched nanostructures (PTB-Pt) with unique catalytic properties, low-density structural stability, multiple electronic effects, high surface area, and maximized atomic utilization can maximize the ORR catalytic activity at low Pt content. This review provides broad and balanced insights on the substantial progress on the rational design of porous PTB-Pt for ORR and their fundamental mechanisms besides the current challenges and perspectives on designing ideal PTB-Pt catalysts for efficient ORR and guidance for future development of real-device.

1. Introduction

The Oxygen reduction reaction (ORR) at the cathodes of the proton-exchange membrane fuel cell (PEMFC) and the metal-air battery is highly promising efficient, green, and sustainable energy sources due to the earth-abundance of oxygen, low-cost, and high-energy output.[1–5] However, these devices remain commercially impractical in automobiles, and light-duty vehicles due to the sluggish ORR kinetics and the high cost of Pt-catalyst that is the indispensable core component in PEMFC (Fig. 1a). [1–4] Various efforts are dedicated to solving these barriers, like engineering morphology, size, and composition of Pt-based catalysts [6–9], besides discovering Pt-free catalysts.[10–16]

Porous ternary Pt-based branched nanostructures, PTB-Pt, (i.e., multipod, dendrites, and flowers) combined unique structural merits (i.e., great surface area, low density, and rich edges/corner), and compositional properties (i.e., prober surface energy and synergistic effects).[17,18] Also, modulation of the d-band center of Pt with two metals allows tunable and facile adsorption and desorption of ORR reactants and intermediates.[19] Nonetheless, tailored synthesis of porous PTB-Pt is complex due to various interdependent interactions of constituents (i.e., reduction of multiple metals with disparate reduction potentials and their mutual interaction with the surfactants). The research related to PTB-Pt increased reached ~ 430 articles, including ~ 156 articles of branched Pt shapes and ~ 30 for ORR according to the Web of Science (2010–2021) (Fig. 1b), so it is utterly necessary to provide timely updates of this field. Some excellent reviews highlighted ternary Pt for ORR in acidic media [20], metal branched nanostructures[17], and porous Pt for electrochemical applications[18]. However, the reviews about PTB-Pt for ORR are not yet addressed as far as we found.

This review emphasizes the rational design of PTB-Pt for ORR, rooting from the fabrication methods and their related mechanisms to qualitative analysis on salient features of ORR beside the current challenges and perspectives direction to develop ideal PTB-Pt for ORR.

2. ORR pathways & mechanisms

The ORR can follow the 4, 2, and 1-electron pathways (Fig. 2a). The ORR mechanism in 4-electron in the acidic electrolyte, including electrocatalytic reduction of O_2 and combined with H to form H_2O at the ideal standard potential (E°) of 1.229 V.[21] In the 2-electron pathway, O_2 is reduced to H_2O_2 and then to H_2O at E° of 1.76 V, which is not favored, due to its lower output current and catalyst poisoning but its widely used in the industry to produce H_2O_2. The 1-electron pathway is essential in understanding the ORR mechanism.

The potential bias and the energy levels for ORR with different transition states are the main parameters to decipher the ORR mechanism, which all involve the adsorbed OOH*, OH*, and HOOH* species (Fig. 2b).[22] Mechanism 1 includes O_2 adsorption and its O-O splitting

* Corresponding author.
E-mail address: Kamel.eid@qu.edu.qa (K. Eid).

https://doi.org/10.1016/j.elecom.2022.107237

Available online 2 February 2022

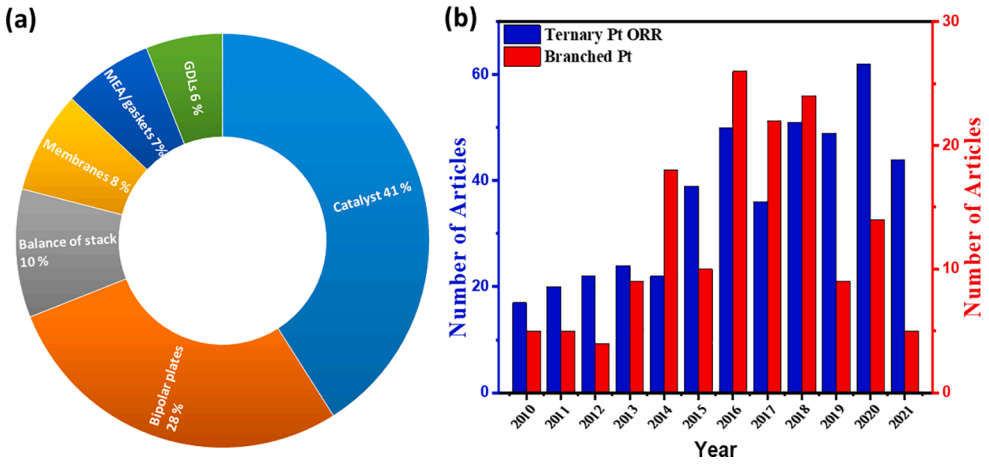

Fig. 1. (a) Components of PEMFC and their costs. (b) Number of articles vs. year of ternary Pt and branched Pt nanostructures published between 2010 and 2021, obtained from Web of Science.

(a)

Electrolyte	ORR Reactions	E°/V
Acidic aqueous solution	$O_2 + 4H^+ + 4e^- \rightarrow H_2O$ (4 electron)	1.229
	$O_2 + 2H^+ + 2e^- \rightarrow H_2O_2$ (2 electron)	0.7
	$H_2O_2 + 2H^+ + 2e^- \rightarrow 2H_2O$	1.76
Alkaline aqueous solution	$O_2 + H_2O + 4e^- \rightarrow 4OH^-$ (4 electron)	0.4
	$O_2 + H_2O + 2e^- \rightarrow HO^- + HO^-_2$ (4 electron) $HO^-_2 + H_2O + 2e^- \rightarrow 3OH^-$ 0.867	0.065
Non-aqueous aprotic solvents	$O_2 + e^- \rightarrow O_2^-$ (1 electron)	Dependent on the electrolyte
	$O_2^- + e^- \rightarrow O_2^{2-}$ (1 electron)	Dependent on the electrolyte

(b)

Mechanism 1	Mechanism 2	Mechanism 3
O_2+* → O_2*	O_2+* → O_2*	O_2+* → O_2*
O_2*+* → 2O*	O_2*+(H^++e^-) → OOH*	O_2*+(H^++e^-) → OOH*
O*+(H^++e^-) → OH*	OOH*+* → O*+OH*	OOH*+(H^++e^-) → HOOH*
OH*+(H^++e^-) → H_2O+*	O*+(H^++e^-) → OH*	HOOH*+* → 2OH*
	OH*+(H^++e^-) → H_2O+*	OH*+(H^++e^-) → H_2O+*

Fig. 2. (a) ORR reactions in various electrolytes and their thermodynamic potentials and (b) ORR mechanisms. Copyrights 2008 Elsevier.[22]

then hydrogenation of atomic O* to OH and then H_2O. Mechanism 2 involves the protonation of O_2 to OOH that dissociates to O and OH, which protonate to OH and H_2O, respectively. In mechanism 3, O_2 is protonated to OOH and then to HOOH, dissociating to OH. Then OH is hydrogenated to H_2O. Mechanism 1 is the most favored among 3-mechanisms, and OH removal is the rate-limiting step at ORR equilibrium potential of 1.23 V.[22] The synergetic effect is preferred for boosting the ORR activity due to its ability to facilitate OH removal, ease proton/electron transfer, and O-O scission.

3. Fabrication mechanisms of PTB-Pt

Pt is easily integrated with two metals to form PTB-Pt using strong or mild reducing agents under mild conditions based on various mechanisms.[17,18,23,24]

3.1. Overgrowth mechanism (OGM)

In OGM, Pt prefers to grow into low-index facets polyhedral shapes, but using proper structural directing agents can form TB-Pt dendrites, thorns, and stars with high-energy facets.[17,24] Mainly, one metal should be initially reduced to form nuclei to serve as seeds for supporting homogeneous or heterogeneous nucleation of other metals followed by subsequent quick atomic addition to form branched shapes.[17] Various PTB-Pt were prepared by OGM like PtNiCo[25], PtPdCu[26], FePtPd[27], PtRuCu[28], and PtAgFe[29], and PtPdCu (ORR).[30] The OGM depends on precursors, seed morphology, reducing agent power, and surfactants, but the effect of these factors on TB-Pt should be optimized.

3.2. Diffusion-limited aggregation (DLA)

In the DLA, the colloidal nanocrystals (NCs) with great interfacial energy and collision frequency coalesce together along a specific crystallographic to usually form nanowires and chains but PTB-Pt shapes could be formed using some surfactants.[17,24] NCs diffuse by Brownian motion, minimize the interfacial energy and provide thermodynamic driving forces for the coalescence and DLA. The weak interaction

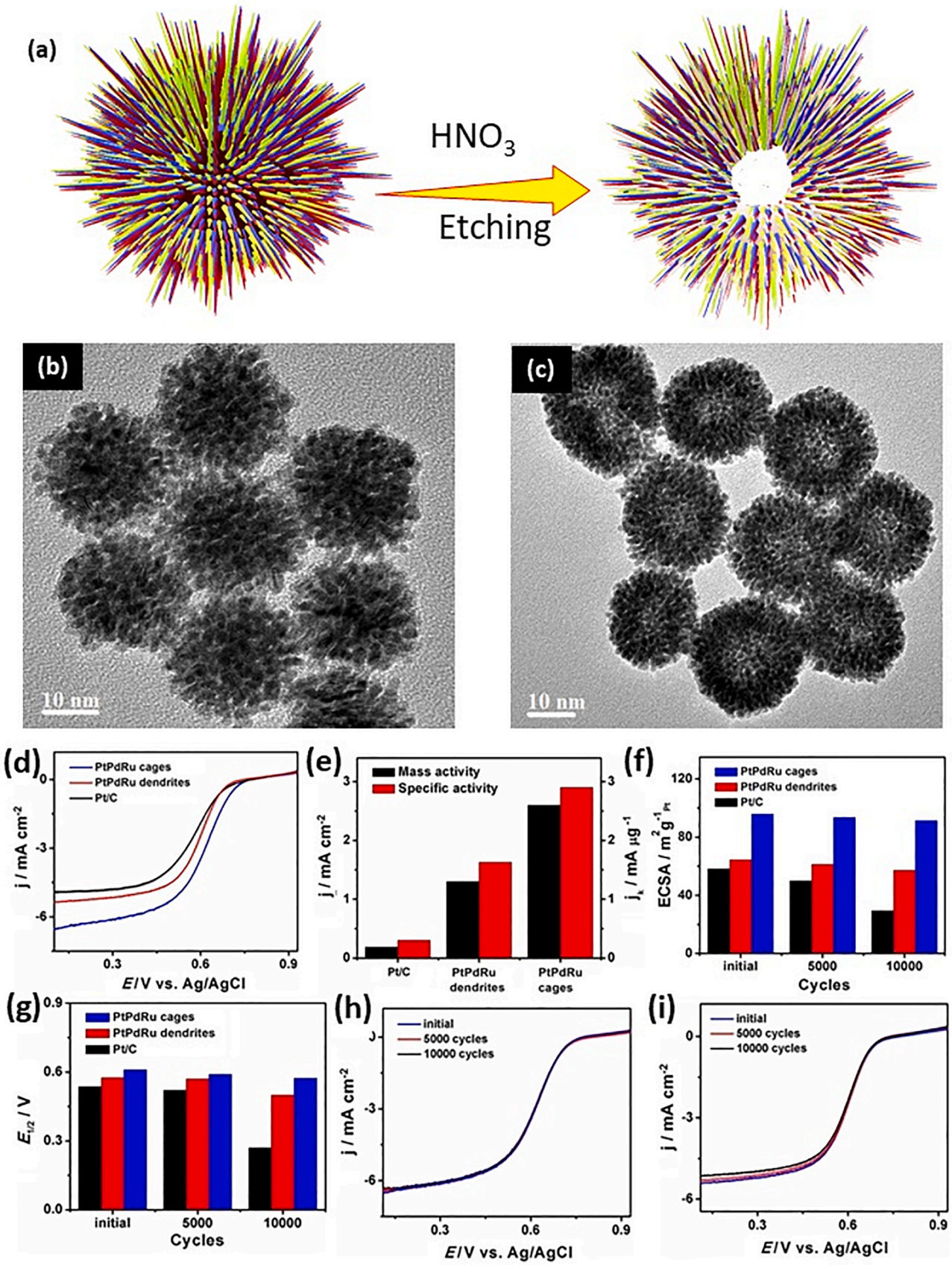

Fig. 3. (a) Preparation scheme of PtPdRu nanocages. TEM image of (b) PtPdRu NDs, (c) PtPdRu nanocages, (d) linear sweep voltammetry (LSV) in O_2-saturated 0.1 M $HClO_4$ at 20 mV s^{-1}, (e) specific/mass activities at 0.6 V, (f) electrochemical active surface area (ECSA), and (g) half-wave potential ($E_{1/2}$). ORR stability of (h) naocages and (i) NDs. Copyrights 2015 ACS.[36]

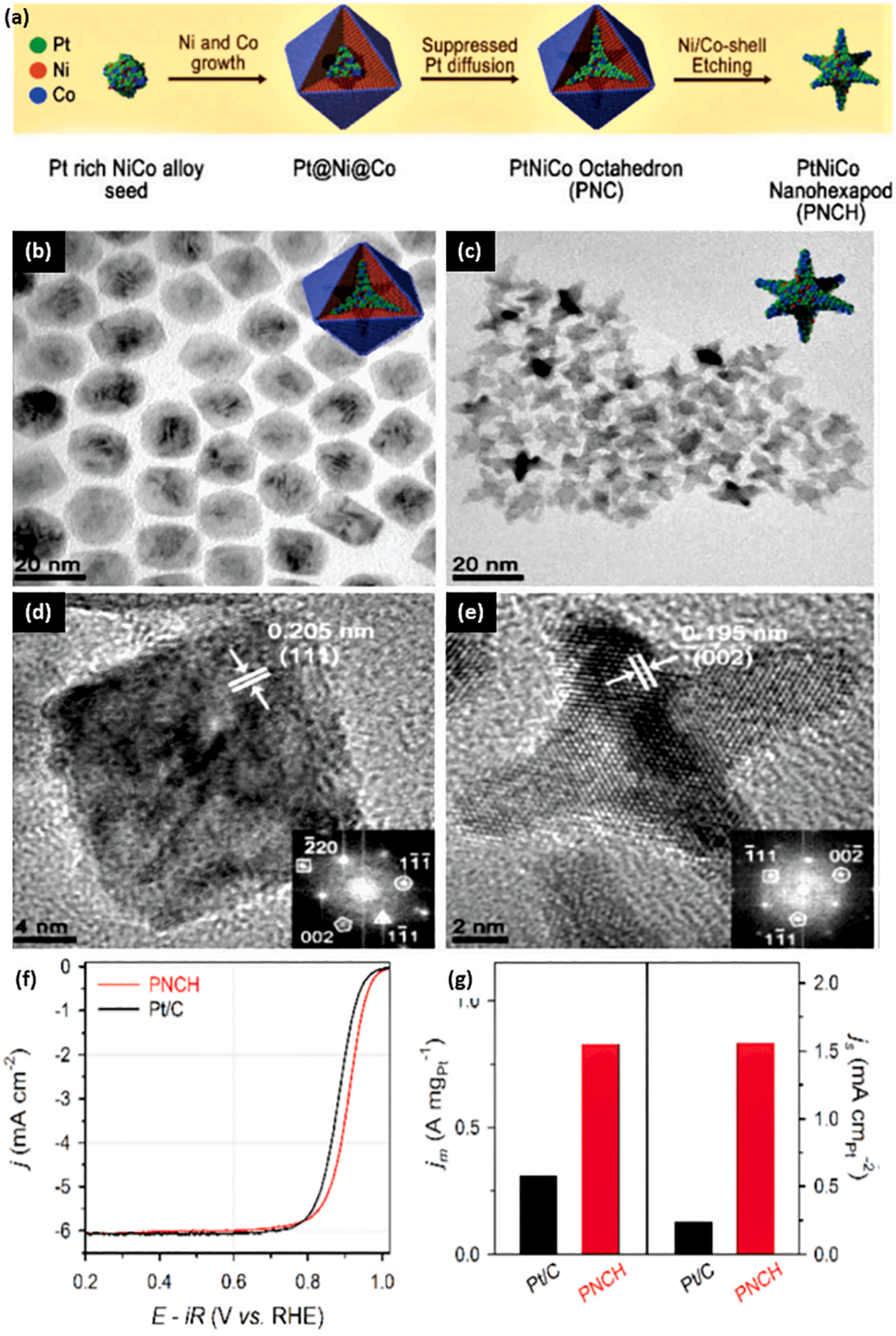

Fig. 4. (a) Formation scheme of PNC and PNCH. TEM image of (b-d) PCN and PNCH (c-e). (f) LSV at 20 mV s^{-1} at 1600 rpm of PNCH and Pt/C and their mass/specific activities at 0.9 V in O_2-saturated 0.1 M $HClO_4$. Copyrights 2016 RSC.[39]

of legend with NCs, high temperature, and strong reduction power promote DLA to form PTB-Pt. Using L-Proline, Triton X-114, oleic acid, and F127 surfactants formed branched PtRuPd[31], PdAuCu[32], and AuPtAg[33]. Notably, the DLA is not studied enough to synthesize TB-Pt.

3.3. Oxidative etching (OEt)

The OEt occurs on edges to transform polyhedral shapes to TB-Pt when the synthesis is conducted under air in the presence of etchants like halides Fe(III), and NH_4OH/H_2O_2.[17,24] The OEt is easily combined with DLA to form Pt(NiCo), Pt(FeNi), and $Pt_3(NiCo)_2$ nanodendrites.[34] In galvanic replacement (GR), one metal with a higher redox potential can reduce or replace the seeded metal. Mainly the cations of the second metal are initially deposited on the surface of the seeded metal to allow electron transfer from seed to metal, then the positively charged ions of the seed migrate away from the deposition sites and diffuse into solution. The dissolution initiates from the high surface-energy facet of seeded metals, but deposition occurs on the low

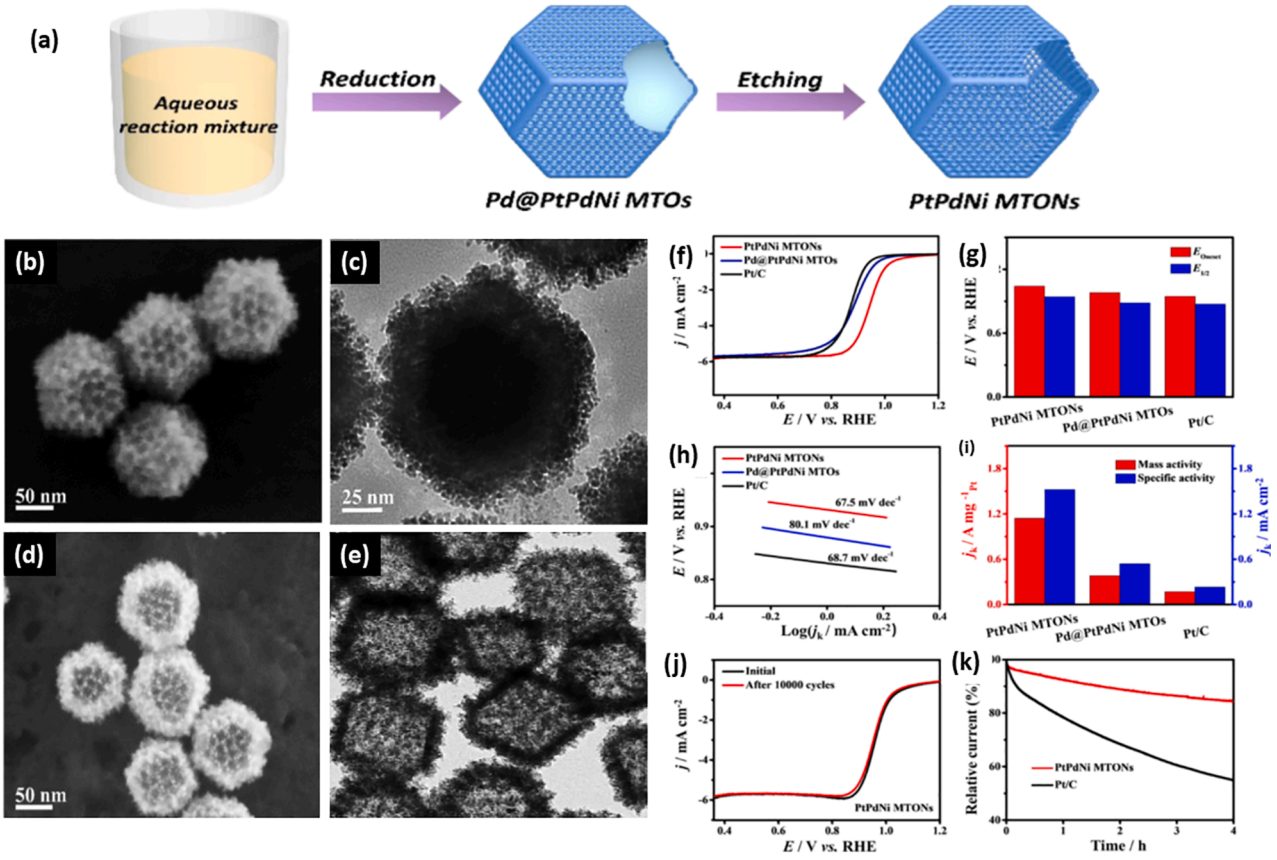

Fig. 5. (a) Formation scheme of MTONs and MTOs. (b) SEM, (c) TEM of MTOs. (d) SEM and (e) TEM of MTONs (f) LSV at 5 mV/s, (g) $E_{1/2}$, (h) Tafel plot, and (i) MA/SA at 0.9 V of MTONS, MTOs, and Pt/C. (j) LSV stability and (k) chronoamperometry stability of MTONs in 0.1 M $HClO_4$. Copyrights 2019 ACS.[44]

surface energy facet. The surfactants tune the deposition and dissolution process to form branched shapes with desired facets.

3.4. *Template-based synthesis*

Ionic/non-ionic copolymer and lyotropic liquid crystals (LLC) are adsorbed on metal atoms during nucleation via a specific functional group and self-assembled into micelles that serve as templates to form PTB-Pt with controlled porosity, pore-volume, and branches.[17,24] The nucleation is naturally isolated from the growth step, resulting in uniform porous branched shapes. The template method works on a small scale, at mild heating, and the template is involved in the reaction and porosity, and branches depend on the template type.

4. Pt-ternary nanodendrites (NDs)

Eid et al. rationally designed PtPdRu NDs (22 nm) with open branches (2–4 nm) by the reduction of Na_2PdCl_4, K_2PtCl_4, $RuCl_3$ by ascorbic acid (AA) (0.4 M) in pluronic F127 solution at 25 °C.[35] The formation mechanism is based on isolation of nucleation from growth step driven by dissimilar reduction kinetics of 3-metals. Pd is initially reduced to act as seeds and provide multisite for deposition of Pt and Ru; meanwhile, pluronic F127 is adsorbed on the PtPdRu nuclei with its poly (propylene oxide) group to assembly into a dendritic structure. The ORR activity of PtPdRu NDs was higher than PtPd nanoflowers and commercial Pt/C catalyst at the same Pt loading beside high stability for 5 K cycles.[35] The same method was used to form PtPdRu NDs but using poly(vinylpyrrolidone) (PVP) (Fig. 3a) with a surface area of (94.5 $m^2 g^{-1}$) followed by soaking in HNO_3 to form PtPdRu nanocage with branched structure and high surface area (179 $m^2 g^{-1}$). The mechanism includes adsorption of PVP via pyrrolidone ring or carbonyl group to form NDs and selective etching power of HNO_3 towards Pd to form nanocage, and the cage size depends on Pd content (Fig. 3c).[36]

The ORR activity of PtPdRu nanocages was higher than PtPdRu NDs and Pt/C (Fig. 3d-i).[36] The mass activity (MA) of PtPdRu nanocages (2.61 mA μg^{-1}) was 2.08 and 14.1 times greater than PtPdRu NDs (1.25 mA μg^{-1}) and Pt/C (0.185 mA μg^{-1}), respectively (Fig. 3e). PtPdRu nanocage outperformed PtFeCu nanorods (0.222 mA μg^{-1}), PtPdBi nanowires (1.16 mA μg^{-1}), and PtPdBi nanospheres (0.67 mA μg^{-1}). After 10 K cycles, $E_{1/2}$ PtPdRu nanocages degraded only by 3.7 mV, due to stable ECSA and nanocage shape (Fig. 3g-i). Au@PtNi NDs formed by reduction of metal salts by AA in Brij 58 solution and then heating at 60 °C for 1 h showed ORR MA (0.538 A mg^{-1}) that was higher than Au@Pt (0.335 A mg^{-1}) and Pt/C (0.428 A mg^{-1}) at 0.80 V beside a greater stability for 10 K cycles, due to trimetals and NDs shape.[37] PtNiIr/C NDs formed by the hydrothermal method at 230 °C showed ORR specific activity (SA) (1.58 mA cm^{-2}) 7-times higher than Pt/C.[38] Although the MA and SA of PtNiIr/C were close to PtNi/C, it showed only a 5.5 % activity loss after 12 K cycles compared to PtNi/C (24 %) and Pt/C (53.2%), implying the better durability of ternary than metal than binary metal. Pt@Ni@Co nanohexapod (PNCH) was prepared by HNO_3 etching of Pt@Ni@Co octahedral (PNC) for boosting ORR (Fig. 4a).[39] $CoCl_2$ slows down the growth of PtNi NCs and suppresses Pt diffusion, and HNO_3 etches Pd to form hexapods. [39] PNC had an octahedral shape (~20 nm size), lattice space (0.205 nm), and shell of Co and Ni (Fig. 4b-d), while PNCH had a nanohexapod shape (~15 nm size) and lattice space (0.195 nm) (Fig. 4c-e).[39] The MA (0.8 A mg^{-1}_{Pt}) and SA (1.6 mA cm^{-1}_{Pt}) of PNCH were 2.7 and 6.5 times higher than Pt/C, respectively, due to branched shape, alloying effect, and stable ECSA (Fig. 4f-g).[39] $Pd_{80}Cu_6Pt_{14}$ NDs formed by reducing Pd, Cu, and Pt by AA in pluronic F127 solution containing HCl at 90 °C enhanced the ORR MA (1.73 A mg^{-1}_{Pt}) 14 times than Pt/C and

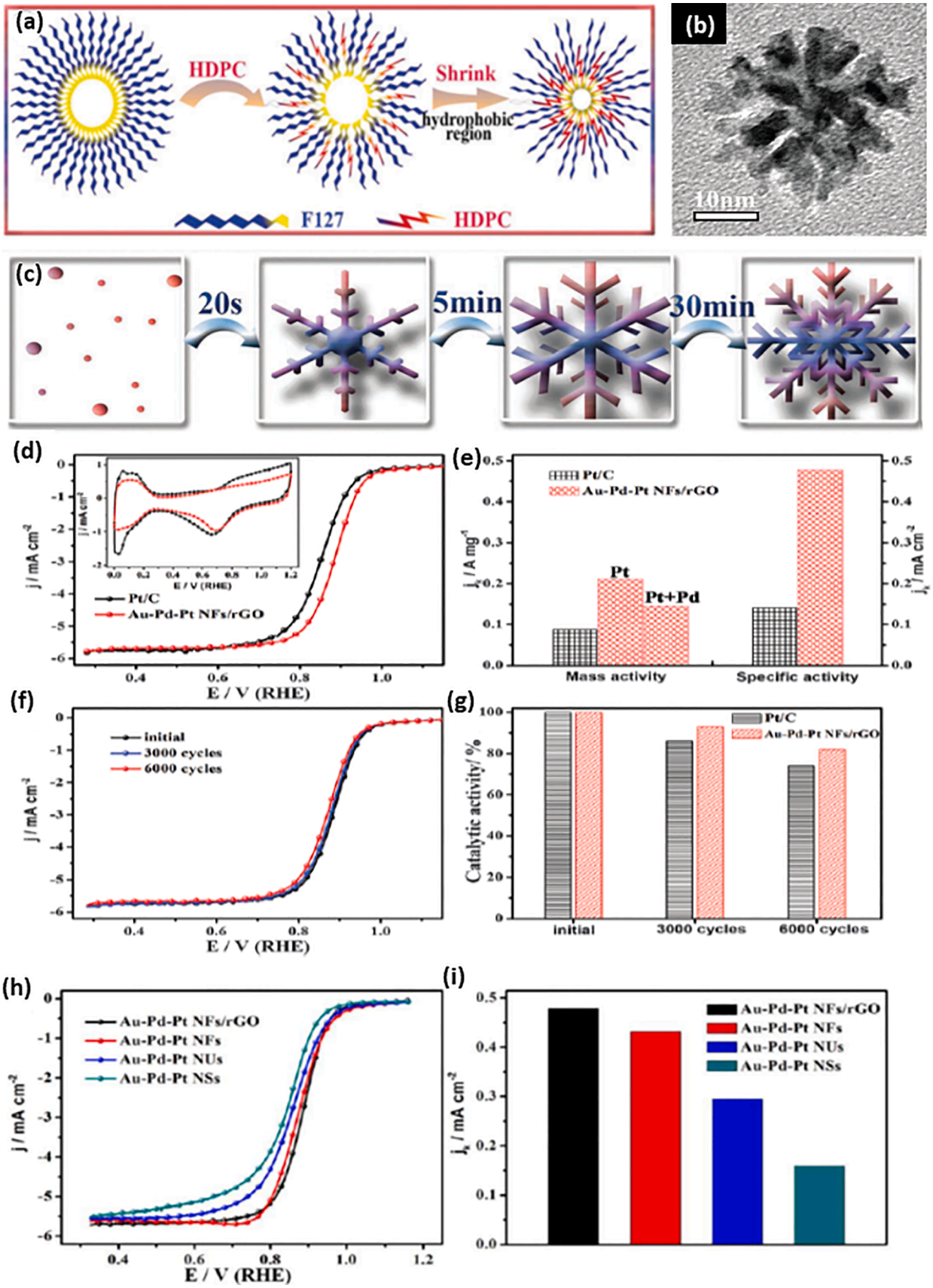

Fig. 6. (a) Synthesis scheme, (b) TEM image, and (c) formation mechanism of Au-Pd-Pt NFs. (d) LSV at 10 mV s^{-1} (CV is in inset), (e) MA/SA at 0.9 V and (f) LSV stability of Au-Pd-Pt NFs/rGO. (g) stability of catalsyst. (h) and (i) ORR activity of Au-Pd-Pt NFs/rGO, NFs, NUs, and NSs. Copyrights 2016 RSC.[46]

durability for 5 K cycles.[40] F127 acts as a template while HCl tunes the reduction power of AA and acts as a facet directing agent to form NDs.

$Pt_3(NiCo)_2$ formed by DLA mechanism using $Fe(acac)_3$ to control the nucleation and crystal overgrowth of NDs revealed ORR MA 10 times higher than Pt/C and greater durability due to the higher surface area and ternary composition.[34] Au@Pt_3Pd NDs formed by the self-assembly gelation strategy showed ORR MA and SA higher than Pt/C and durability for 5 K cycles.[41] The same method was used to prepare PtPdNi mesoporous with a branched surface (MNs)[42] and PtPdCo MNs[43], which both enhanced the ORR activity than PtPdNi NDs, PtPd MNs, and Pt/C, due to porosity and branching that maximize the usage of metals during ORR.

Pd@PtPdNi mesoporous-truncated octahedral (MTOs) was obtained by reduction of Pt, Ni, and Pd salts by AA in pluronic F127 and HCl solution, followed by etching in HNO_3 to form PtPdNi MTOs nanocages (MTONs) (Fig. 5a-e).[44] The mechanism involves the reduction of Pd to act as seeds for supporting add atom of Pt and Ni via isolation growth from nucleation step to form MTOs, while HNO_3 etches Pd to form MTONs. The ORR activity (MA, SA, $E_{1/2}$, and kinetics) and stability of MTONs were higher MTOs and Pt/C, owing to mesopores, branches, and cage shape, which maximize utilization of Pt, Pd, and Ni and accelerate mass transfer during ORR (Fig. 5f-k). The 4-electron pathway is achieved using MTONs. Recently, PtRuPd NDs made by reduction of Pt, Pd, and Ru in hexadecyl pyridinium chloride monohydrate (HDPC) by AA based on Ostwald repining growth mechanism (ORGM) showed ORR MA (1.368 A mg^{-1}) higher than Pt/C (1.1 A mg^{-1}), PdRu NDs (1.159 A mg^{-1}), and PtPd NDs (0.717 A mg^{-1}).[31] This is due to porous NDs shape and alloy Pt with Pd and Ru, which enhance adoption of reactants and reduce binding energy of ORR intermediates. AuPtPd NDs were formed by ORGM in L-proline solution contains NaOH and displayed higher MA (58.49 mA mg^{-1}) than AuPt NCs (39.69 mA mg^{-1}), AuPd NCs (5.97 mA mg^{-1}), Pt blacks (26.68 mA mg^{-1}), and Pd black (22.02 mA mg^{-1}) and durability for 1 K cycles. This is due to the synergetic effect of ternary metals and NDs shape.[45] L-Proline with its α-amino group and α-carboxylic interact strongly with Pt, Pd, and Au, tune the crystal growth kinetics and facilitate ORGM.

5. Ternary Pt-based nanoflowers (NFs)

Au-Pd-Pt NFs/rGO was obtained by the reduction of Au, Pd, and Pt salts by AA in pluronic F127 and HDPC solution, followed by addition of rGO under stirring (Fig. 6).[46] The mechanism involves the self-assembly of pluronic F127 and HDPC to form Au NFs (Fig. 6a-b) that grow into nanowires and act as seeds for supporting deposition of Pd and Pt to yield Au-Pd-Pt NFs/rGO (Fig. 6c). pluronic 123 and brig 58 instead of F127 formed urchin-like (Au-Pd-Pt NUs) and snowflake structure (Au-Pd-Pt NSs). The ORR activity and stability of Au-Pd-Pt NSs/rGO were higher than Au-Pd-Pt NFs, Au-Pd-Pt NUs, Au-Pd-Pt NSs, and Pt/C (Fig. 6d-i). The MA of Au-Pd-Pt NFs/rGO (0.212 A mg^{-1}_{Pt} and 0.145 A mg^{-1}_{PdPt}) was 2.4 and 1.63 times greater than Pt/C beside only 16 % loss after 6 K cycles compared to Pt/C (25 %). This is due to NFs shapes, rGO support, and electronic interaction, enhancing reactants' adsorption and weakening intermediates' adsorption. The ORR pathway includes 4 electrons, and the ORR mechanism includes O_2-activation, protonation, and electron transfer to form OOH before O-O splitting and the adsorbed O and OH formed on Au-Pd-Pt NSs/rGO surface after dissociation. So alloying Pt with Pd/Au lessens the d-band center and Pt and reduces intermediates' binding energy.

Pt-Pd-Ag NFs formed by co-reduction of metal salts by AA in solutions of hexamine enhanced the ORR MA by 17, 22, and 187 times than Pt/C, Pd/C, and Pt-Pd-Ag/C NCs, respectively, and higher stability, due to NFs shape and alloying Pt with Pd/Ag.[47] PtCoNi FNs formed by reducing Pt, Co, and Ni in an ice-bath by KBH_4 enhanced the ORR MA by 1.92, 2.17, and 5.51 fold than PtNi NCs, PtCo NCs, and Pt black, congruently.[48] PtNiCo NFs/C obtained by hydrothermal method followed by heat treatment under N_2/H_2 at 700 °C boosted the ORR SA by 6.74 fold than PtNiCo NCs and 12.35 fold than Pt/C besides higher durability, due to tri-metallic composition and NFs shape.[49] PtNiCo NFs/C outperformed other ternary shapes like wires, cubes, and octahedrons. [49] However, the ORR performance of ternary Pt-based NFs is not studied enough relative to other shapes.

6. Conclusion and prospects

PTB-Pt NDs are relatively more studied than NFs; however, both are not studied enough for ORR compared with other shapes. Chemical reduction by AA in non-ionic copolymers like pluronic F127 and PVP solutions is the most common method for synthesizing PTB-Pt NDs. Using HCl with copolymer can form mesoporous branched PtPdNi MNs, PtPdCo, and Pd@PtPdNi. HNO_3 etching using and chemical reduction formed novel PtPdRu nanocages, and Pt@Ni@Co nanohexapods. The hydrothermal method was used to produce AuPtPd NDs, PtNiIr/C NDs, and Au@Pt_3Pd NDs. PTB-Pt NDs enhanced the ORR than their counterparts binary Pt-based and Pt/C. Various PTB-Pt NFs like Au-Pd-Pt, Pt-Pd-Ag, and PtNiCo/C were formed by chemical reduction or hydrothermal method using hexamine and HDPC with pluronic F127 as a template. PtCoNi FNs were formed by KBH_4 as a reductant without surfactant that is highly promising for large-scale applications. PTB-Pt NFs promoted the ORR than binary Pt-based and Pt/C

For the future perspective, it is crucial to develop facile methods for high-mass production of ternary Pt-system as the current methods are not feasible or the practical applications. Rationally designed PTB-Pt with high yield at room temperature in situ supported to allow their mixing at the atomic level rather than segregation that is useful for augmenting ORR. This could be achieved by combining several approaches, like chemical reduction with template-method. Also, using carbon materials as support for ternary Pt-system can enhance their activity. Using novel materials like MXenes and graphdiyne with their unique catalytic properties can promote the ORR activity of ternary Pt.

CRediT authorship contribution statement

Kamel Eid: Conceptualization, Methodology, Writing – original draft. **Aboubakr M. Abdullah:** Validation, Writing – review & editing.

Declaration of Competing Interest

The authors declare no conflict of interest that could influence the presented work.

Acknowledgments

This work was supported by (i) the Qatar National Research Fund (QNRF, a member of the Qatar Foundation) through a National Priority Research Program Grant (NPRP) NPRP13S-0117-200095 and (ii) Qatar University through an International Research Collaboration Co-Fund grant, IRCC-2021-015. Statements made herein are solely the responsibility of the authors. Open Access funding provided by Qatar National Library.

References

[1] P. Shirvanian, F. van Berkel, Electrochem. Commun. 114 (2020), 106704.
[2] S. Lu, K. Eid, Y. Deng, J. Guo, L. Wang, H. Wang, H. Gu, J. Mater. Chem. A 5 (2017) 9107–9112.
[3] K. Eid, H. Wang, V. Malgras, S.M. Alshehri, T. Ahamad, Y. Yamauchi, L. Wang, J. Electroanal. Chem. 779 (2016) 250–255.
[4] A.K. Ipadeola, A.B. Haruna, L. Gaolatlhe, A.K. Lebechi, J. Meng, Q. Pang, K. Eid, A. Abdullah, K.I. Ozoemena, ChemElectroChem. 8 (2021) 3998–4018.
[5] A.K. Ipadeola, P.V. Mwonga, K.I. Ozoemena, Electrochim. Acta 390 (2021), 138860.
[6] V. Mashindi, P. Mente, N. Mpofu, T.N. Phaahlamohlaka, O. Makgae, A.I. Kirkland, R. Forbes, K.I. Ozoemena, P.B. Levecque, N.J. Coville, J. Appl. Electrochem. (2021) 1–18.
[7] H. Zhang, H. Wang, K. Eid, L. Wang, Part. Part. Syst. Char. 32 (2015) 863–868.

[8] H. Wang, S. Yin, K. Eid, Y. Li, Y. Xu, X. Li, H. Xue, L. Wang, ACS Sustainable Chem. Eng. 6 (2018) 11768–11774.
[9] L. Huang, Y.Q. Su, R. Qi, D. Dang, Y. Qin, S. Xi, S. Zaman, B. You, S. Ding, B.Y. Xia, Angew. Chem. Int. Ed. 60 (2021) 25530–25537.
[10] M.A. Ahsan, T. He, K. Eid, A.M. Abdullah, M.L. Curry, A. Du, A.R. Puente Santiago, L. Echegoyen, J.C. Noveron, J. Am. Chem. Soc. 143 (2021) 1203–1215.
[11] C. Wei, H. Wang, K. Eid, J. Kim, J.H. Kim, Z.A. Alothman, Y. Yamauchi, L. Wang, Chemistry-A European Journal 23 (2017) 637–643.
[12] F. Ando, T. Gunji, T. Tanabe, I. Fukano, H.C.D. Abruña, J. Wu, T. Ohsaka, F. Matsumoto, ACS Catal. 11 (2021) 9317–9332.
[13] J. Min, X. Xu, J.J. Koh, J. Gong, X. Chen, J. Azadmanjiri, F. Zhang, X. Wen, C. He, ACS Applied Energy Materials 4 (2021) 3317–3326.
[14] Q. Li, Y. Chen, F. Du, X. Cui, L. Dai, Appl. Catal. B 304 (2022), 120959.
[15] F. Dong, M. Wu, Z. Chen, X. Liu, G. Zhang, J. Qiao, S. Sun, Nano-Micro Letters 14 (2022) 1–25.
[16] M.A. Ahsan, T. He, K. Eid, A.M. Abdullah, M.F. Sanad, A. Aldalbahi, B. Alvarado-Tenorio, A. Du, A.R. Puente Santiago, J.C. Noveron, ACS Appl. Mater. Interfaces 14 (2022) 3919–3929.
[17] B. Lim, Y. Xia, Angew. Chem. Int. Ed. 50 (2011) 76–85.
[18] Y. Xu, B. Zhang, Chem. Soc. Rev. 43 (2014) 2439–2450.
[19] M. Torihata, M. Nakamura, N. Todoroki, T. Wadayama, N. Hoshi, Electrochem. Commun. 125 (2021), 107007.
[20] J. Kim, Y. Hong, K. Lee, J.Y. Kim, Adv. Energy Mater. 10 (2020) 2002049.
[21] W. Chen, J. Huang, J. Wei, D. Zhou, J. Cai, Z.-D. He, Y.-X. Chen, Electrochem. Commun. 96 (2018) 71–76.
[22] A.U. Nilekar, M. Mavrikakis, Surf. Sci. 602 (2008) L89–L94.
[23] K. Eid, H. Wang, V. Malgras, Z.A. Alothman, Y. Yamauchi, L. Wang, Chemistry-An Asian Journal 11 (2016) 1388–1393.
[24] C. Zhu, D. Du, A. Eychmüller, Y. Lin, Chem. Rev. 115 (2015) 8896–8943.
[25] H.-Y. Chen, H.-J. Niu, Z. Han, J.-J. Feng, H. Huang, A.-J. Wang, J. Colloid Interface Sci. 570 (2020) 205–211.
[26] N. Gao, X. Wu, X. Li, J. Huang, D. Li, D. Yang, H. Zhang, RSC Adv. 10 (2020) 12689–12694.
[27] D. Ung, L.D. Tung, G. Caruntu, D. Delaportas, I. Alexandrou, I.A. Prior, N.T. Thanh, CrystEngComm 11 (2009) 1309–1316.
[28] S. Xue, W. Deng, F. Yang, J. Yang, I.S. Amiinu, D. He, H. Tang, S. Mu, ACS Catal. 8 (2018) 7578–7584.
[29] A. Mahmood, H. Lin, N. Xie, X. Wang, Chem. Mater. 29 (2017) 6329–6335.
[30] H. Wang, S. Yin, Y. Xu, X. Li, A.A. Alshehri, Y. Yamauchi, H. Xue, Y.V. Kaneti, L. Wang, J. Mater. Chem. A 6 (2018) 8662–8668.
[31] J.-J. Duan, X.-X. Zheng, H.-J. Niu, J.-J. Feng, Q.-L. Zhang, H. Huang, A.-J. Wang, J. Colloid Interface Sci. 560 (2020) 467–474.
[32] Y. Chen, A.-J. Wang, P.-X. Yuan, X. Luo, Y. Xue, J.-J. Feng, Biosens. Bioelectron. 132 (2019) 294–301.
[33] Y.-C. Shi, A.-J. Wang, P.-X. Yuan, L. Zhang, X. Luo, J.-J. Feng, Biosens. Bioelectron. 111 (2018) 47–51.
[34] G.M. Leteba, D.R. Mitchell, P.B. Levecque, C.I. Lang, Nanomaterials 8 (2018) 462.
[35] K. Eid, V. Malgras, P. He, K. Wang, A. Aldalbahi, S.M. Alshehri, Y. Yamauchi, L. Wang, RSC Adv. 5 (2015) 31147–31152.
[36] K. Eid, H. Wang, V. Malgras, Z.A. Alothman, Y. Yamauchi, L. Wang, The Journal of Physical Chemistry C 119 (2015) 19947–19953.
[37] Q. Shi, C. Zhu, S. Fu, D. Du, Y. Lin, ACS Appl. Mater. Interfaces 8 (2016) 4739–4744.
[38] T. Yang, Y. Ma, Q. Huang, M. He, G. Cao, X. Sun, D. Zhang, M. Wang, H. Zhao, Z. Tong, ACS Appl. Mater. Interfaces 8 (2016) 23646–23654.
[39] A. Oh, Y.J. Sa, H. Hwang, H. Baik, J. Kim, B. Kim, S.H. Joo, K. Lee, Nanoscale 8 (2016) 16379–16386.
[40] S. Fu, C. Zhu, J. Song, P. Zhang, M.H. Engelhard, H. Xia, D. Du, Y. Lin, Nanoscale 9 (2017) 1279–1284.
[41] Q. Shi, C. Zhu, Y. Li, H. Xia, M.H. Engelhard, S. Fu, D. Du, Y. Lin, Chem. Mater. 28 (2016) 7928–7934.
[42] C. Li, Y. Xu, Y. Li, H. Yu, S. Yin, H. Xue, X. Li, H. Wang, L. Wang, Green Energy Environ. 3 (2018) 352–359.
[43] C. Li, Y. Xu, Y. Li, H. Xue, Z. Wang, X. Li, L. Wang, H. Wang, Chemistry–An Asian Journal 13 (2018) 2939–2946.
[44] H. Wang, Y. Li, K. Deng, C. Li, H. Xue, Z. Wang, X. Li, Y. Xu, L. Wang, ACS Appl. Mater. Interfaces 11 (2019) 4252–4257.
[45] H.-Y. Chen, A.-J. Wang, L. Zhang, J. Yuan, Q.-L. Zhang, J.-J. Feng, Int. J. Hydrogen Energy 43 (2018) 22187–22194.
[46] L. Huang, Y. Han, S. Dong, Chem. Commun. 52 (2016) 8659–8662.
[47] A. Chalgin, F. Shi, F. Li, Q. Xiang, W. Chen, C. Song, P. Tao, W. Shang, T. Deng, J. Wu, CrystEngComm 19 (2017) 6964–6971.
[48] M.-T. Liu, L.-X. Chen, A.-J. Wang, K.-M. Fang, J.-J. Feng, Int. J. Hydrogen Energy 42 (2017) 25277–25284.
[49] M. Lokanathan, I.M. Patil, B. Kakade, Int. J. Hydrogen Energy 43 (2018) 8983–8990.